doi:10.1038/nature23001

Methods

Manuscript references[1–22]

Cell culture, fixation and sorting

Two mouse ESC lines were used. One diploid F1 hybrid ESC from an intercross of Mus musculus 129/SV-Jae and Mus musculus castaneus (129 x Castaneus, a gift from Joost Gribnau) and one haploid ESC[23] (H129-1; ECACC 14040203, gift from Martin Leeb and Anton Wutz) were grown either in 2i medium without feeder cells or ES-DMEM with fetal bovine serum (FBS) on feeder cells[24]. Both cell lines were tested for mycoplasma contamination. For harvesting ESCs from cultures on feeder cells, the feeder cells were depleted using Feeder Removal MicroBeads (Miltenyi Biotec), followed by fixation and permeabilisation of the enriched ESCs and staining for Oct-3/4-immunoreactivity as described below. Oct-3/4-positive cells were collected by Fluorescence-activated cell sorting (FACS), ready for subsequent Hi-C processing.

To fix the cells, 50 to 200 million ESCs were suspended in relevant medium and fixed for 10 min by adding formaldehyde at a final concentration of 2% at room temperature before quenching with 127 mM glycine for 5 min on ice. The cells were washed with PBS and permeabilised in 10 mM Tris-HCl (pH 8), 10 mM NaCl, 0.2% IGEPAL CA-630 with cOmplete EDTA-free protease inhibitor cocktail (Roche) for 30 min on ice with intermittent agitation, and spun to collect the nuclei pellet, which was ready for Hi-C processing.

To enrich for specific cell types before the Hi-C process, cells were blocked with PBS-FT (5% FBS, 0.1% Tween-20 in PBS) at room temperature for 1 hr, incubated with a primary antibody in PBS-FT as required (anti-Oct3/4, Santa-Cruz sc-5279, at 1:100 dilution; or anti-Geminin, Abcam 175799 at 1:400 dilution) for 1 hr on ice. Samples were then washed with PBS-FT, and incubated with the secondary antibodies (Alexa Fluor 647-anti-mouse IgG, Thermo Fisher A-31571, or Alexa Fluor 555-anti-rabbit IgG, Thermo Fisher A-21428) for 30 min on ice, washed with 2% FBS in PBS, stained with Hoechst 33342 at the final concentration of 15 μg/ml and subjected to FACS by Influx (BD Biosciences) to collect nuclei cells of interest.

For some diploid cells (batch id = 27 to 35 in **Extended Data Fig. 1i**), the same labelling procedure with anti-Geminin antibody and Hoechst 33342 was applied after Hi-C processing. Then Geminin-immunoreactivity and DNA content of individual single cells were recorded during FACS into 96-well plates.

Hi-C processing

The cells (approximately half million to several million) were washed with 1.24 x NEBuffer 3 (New England Biolabs; 62 mM Tris-HCl [pH 7.9], 124 mM NaCl, 12.4 mM $MgCl_2$, 1.24 mM DTT) and suspended in 400 µl of 1.24 x NEBuffer 3. Six µl of 20% SDS was added and incubated at 37˚C for 60 min with constant agitation, then 40 µl of 20% Triton X-100 was added and incubated at 37˚C for 60 min with constant agitation. Next, 50 µl of 25 U/µl Mbo I (New England Biolabs) was added and incubated at 37˚C overnight with constant agitation. To label the digested DNA ends, 1.56 µl of 10 mM dCTP, 1.56 µl of 10 mM dGTP, 1.56 µl of 10 mM dTTP, 39 µl of 0.4 mM biotin-14-dATP (Thermo Fisher) and 10.4 µl of 5 U/µl DNA polymerase I, large (Klenow) fragment (New England Biolabs) were added and incubated at 37˚C for 45 min with occasional mixing. The sample was then spun and supernatant partially removed leaving 50 µl with cells, followed by addition of 100 µl of 10x T4 DNA ligase reaction buffer (New England Biolabs), 10 µl of 100x BSA (New England Biolabs), water and 10 µl of 1 U/µl T4 DNA ligase (Thermo Fisher) were added to make the total volume 1 ml, and incubated at 16˚C overnight. Then the nuclei were passed through a 30 µm cell strainer and single nuclei were sorted into individual empty wells in 96 well plates using an Influx cell sorter. The plates were sealed and stored at -80˚C until further processing.

Single-cell Hi-C library preparation

To prepare single-cell Hi-C libraries from single nuclei in a 96 well plate, 5 µl of PBS was added to each well, the plate was sealed and crosslinks reversed by incubating at 65˚C overnight. Hi-C concatemer DNA was fragmented and linked with sequencing adapters using the Nextera XT DNA Library Preparation Kit (Illumina), by adding 10 µl of Tagment DNA Buffer and 5 µl of Amplicon Tagment Mix, incubating at 55˚C for 5 min, then cooling down to 10˚C, followed by addition 5 µl of Neutralize Tagment Buffer and incubation for 5 min at room temperature. Hi-C ligation junctions were then captured by Dynabeads M-280 streptavidin beads (Thermo Fisher; 20 µl of original suspension per single-cell sample). Beads were prepared by washing with 1 x BW buffer (5 mM Tris-Cl pH 7.5, 0.5 mM EDTA, 1 M NaCl), resuspended in 4 x BW buffer (20 mM Tris-Cl pH 7.5, 2 mM EDTA, 4 M NaCl; 8 µl per sample), and then mixed with the 25 µl sample and incubated at room temperature overnight with gentle agitation. Using a Bravo automated liquid handling system (Agilent Technologies), the beads were then washed four times with 200 µl of 1 x BW buffer, twice with 200 µl of 10 mM Tris-Cl pH 7.5 at room temperature, and resuspended in 25 µl of 10 mM Tris-Cl pH 7.5. Single-cell Hi-C libraries were amplified from the beads by adding 15 µl of Nextera PCR Master Mix, 5 µl of Index 1 primer of choice and 5 µl of Index 2 primer of choice. Samples were then incubated at 72˚C for 3 min, 95˚C for 30 sec followed by the thermal cycling at 95˚C for 10 sec, 55˚C for 30 sec and 72˚C for 30 sec for 12 or 18 cycles,

then incubated at 72˚C for 5 min. The supernatant was separated from the beads, and the 96 supernatants from a 96 well plate that had 12 cycles of amplification were combined together whereas the supernatants from 18 cycles of amplification were processed uncombined. The combined or uncombined supernatant was purified with AMPure XP beads (Beckman Coulter; 0.6 times volume of the supernatant) according to manufacturer's instructions and eluted with 10 mM Tris-Cl pH 8.5 (100 µl when 96 samples were combined; 30 µl when sample was uncombined). The eluate was purified once more with AMPure XP beads (equal volume to the previous eluate) and eluted with 11 µl of 10 mM Tris-Cl pH 8.5.

Strand-specific nuclear RNA-seq library preparation

Ten to 20 million unfixed ESCs (grown in 2i medium without feeder cells) were washed with cold PBS, resuspended in 0.5 ml of cold buffer RLN (50 mM Tris pH 7.5, 140 mM NaCl, 1.5 mM $MgCl_2$, 1 mM DTT, 0.4% IGEPAL CA-630) and incubated for 5 min on ice. The samples were spun and the resultant pellets (nuclei) were washed with buffer RLN and subject to RNA isolation using RNeasy Mini Kit (Qiagen) and QIAshredder spin columns (Qiagen) according to the instructions from the manufacturer. The strand-specific RNA-seq libraries were prepared from 200 ng each of nuclear RNA samples using TruSeq Stranded Total RNA LT Sample Prep Kit (Illumina) according to manufacturer's instructions.

library QC and sequencing

Before sequencing, the libraries were quantified by qPCR (Kapa Biosystems) and the size distribution was assessed with Agilent 2100 Bioanalyzer (Agilent Technologies). They were sequenced by either 2 x 50 bp, 2 x 75 bp or 2 x 150 bp paired-end run by HiSeq 1500, HiSeq 2500 or NextSeq 500 (Illumina).

Sequence processing pipeline

Paired-end reads of sequencing batches were de-multiplexed to single-cell datasets based on the two 8 bp unique identification tags attached to each cell sample during library amplification. Reads lacking a perfect match were discarded. Reads were broken down to segments on their matches to the MboI recognition site (GATC), concatenating segments shorter than 16 bp with their adjacent segment. Each segment was independently mapped to the *Mus Musculus* genome (assembly mm9) Using Bowtie2[25] in *end-to-end* alignment mode. The uniquely mapped (MAPQ > 36) segments from each paired-end read were consolidated into a chain of segments by merging segments mapped to overlapping genomic regions. Next, the segments chain was translated to a chain of fragment-ends (fends) by associating each segment with its downstream fend. Finally, adjacent fend pairs

from all chains were used to comprise the contact map of the cell. For the single-cell analysis, we used the distinct contacts in each cell, ignoring the number of times each contact appeared in the map. When analysing pooled contact maps we also considered the number of times each contact appeared.

Quality controls and selection of high quality contact maps

We calculated several metrics to evaluate the quality of each contact map:

1. *Coverage*: Total number of contacts
2. *Trans fraction*: Fraction of inter-chromosomal contacts out of the total number of contacts
3. *Non-digested fraction*: fraction of contacts between fends distanced less than 1 kb from each other out of the total number of contacts. The vast majority of these ultra-close cis contacts originate from non-digested DNA and therefore this metric quantifies the digestion efficiency of the experiment.
4. *Max chromosomal coverage aberration*: We calculated coverage enrichment per chromosome and cell by comparing the number of contacts a chromosome forms with the expected number given the mean fraction of contacts per chromosome across the entire single cell pool. The *max chromosomal coverage aberration* of a cell is the maximal enrichment (or depletion) of this log2-ratio across all its chromosomes.
5. *Strongest contact decay bin*: The contact distance bin with the most contacts (see below for definition of the logarithmic decay bins)

The following filters were applied on the contact maps to select high quality ones:

Metric	**Diploid condition**	**Haploid condition**
Coverage	20K-700K	10K-1M
Trans fraction	< 15%	< 20%
Non-digested fraction	< 55%	< 50%
Max chromosomal coverage aberration	½ to 2	½ to 2
Strongest contact decay bin	> 45 (46 kb)	> 45 (46 kb)

We found no systematic technical differences between 2i- and serum- cultured cells **(Extended Data Figs. 1h-j and 8a-c**), so we applied the same quality control filters for both. For the diploid analysis we only used 2i-cultured cells.

In our previous version of the single-cell Hi-C protocol[12] we found that molecules supported by a single read (singleton contacts) usually represented spurious ligations and were therefore discarded. In contrast, the improved single cell Hi-C approach shows no

significant difference in QC metrics between singly and doubly covered molecules (represented as segment chains in the processing pipeline). For example, we found that singleton chains have the same cis to trans ratio as multiply covered chains (mean of 93% versus 92.9%), suggesting low level of spurious contacts is represented in both classes. We note that in addition to overall improved processing robustness and quality, the sequencing depth of our current libraries, in contrast to the previous version, is usually far from saturation (**Extended Data Fig. 1b-c**) so the fraction of singleton chains is much higher (mean 21%, **Extended Data Fig. 1a**).

Repli-score and time of replication analysis

Repli-score quantifies the coverage enrichment of early replicating regions over late replicating ones. To calculate it we characterized each fend by the mean Repli-chip value around it (10Kb upstream and downstream), using replicate 1 of the *Mus Musculus* 129 ES-D3 Repli-chip dataset[15]. Repli-chip values are bimodal around zero, with early replicating loci having positive values and late loci negative ones. The repli-score of a cell is the frequency of early replicating fends in its contact map, divided by the minimal frequency found across all QC passed cells (to scale the score to be relative to one).

The generation of ordered correlation matrix of normalized domain copy-number (**Extended Data Fig. 4c**) is very sensitive to chromosomal copy-number variations. Therefore we selected cells with strictly normal chromosomal coverage (cells with *max chromosomal coverage aberration* between 0.82-1.23), ending up using 46% of the cells. We next counted per cell the total number of contacts formed by each domain (*trans* and *cis* above 23.17Kb). Domains without time of replication information and domains with extremely low (< 0.04) or high (> 0.16) mean number of contacts per Kb (4.8% of the domains) were discarded. The 50 domains with the earliest mean time of replication and the 50 domains with the latest one were marked as top-early and top-late, respectively. Contact numbers were transformed to contact frequencies. The Pearson correlation matrix between all pairs of domains was then calculated, and domains were ordered by their coverage profile mean Pearson correlation with the top-early domains coverage profile minus the mean Pearson correlation with the top-late profiles. The same steps were repeated to order the domains by their A-score instead of by their time of replication (**Extended Data Fig. 10g**) only with ordering the domains by their difference of mean correlation with the 50 domains with highest A-score to their mean correlation with the 50 domains with lowest A-score.

In-silico cell phasing over the cell cycle

We counted the number of *cis* (intra-chromosomal) contacts per cell, binning contacts by distance into logarithmic bins (143 bins, first one for contacts distanced < 1Kb, then each bin covers an exponent step of 0.125, using base 2). Contacts in bins 1-37 were found to be noisy and were discarded, making bins 38-143 the valid bins. The following metrics were used to phase the cells:

- *% near* - percentage of contacts in bins 38-89 out of all valid bins
- *% mitotic* – percentage of contacts in bins 90-109 out of all valid bins
- *farAvgDist* – mean contact distance considering bins >= 98
- *rawRepliScore* – fraction of early-replicating fends out of all fends in the contact map (see above for details)

Each cell was assigned to a group and cells within each group were ordered by these criteria (scale means subtracting the mean and dividing by the standard deviation):

Group	Typical phase	Assignment Criteria		Ordering by
		Diploid cells	Haploid cells	
1	Post-M	$\%\ mitotic \geq 30 \wedge \%\ near \leq 50$	$\%\ mitotic \geq 30 \wedge \%\ near \leq 42$	$-\%\ mitotic$
2	G1	$\%near \leq 63$	$\%\ near \leq 61.1$	$scale(\%\ near) + scale(farAvgDist)$
3	Early to mid-S	$63 < \%\ near \leq 78.5$	$61.1 < \%\ near \leq 77$	$\frac{\%\ near}{VAR(\%\ near)} + \frac{rawRepliScore}{VAR(rawRepliScore)}$
4	Mid-S to G2	$\%\ near > 78.5$	$\%\ near > 77$	$\frac{\%\ near}{VAR(\%\ near)} - \frac{rawRepliScore}{VAR(rawRepliScore)}$
5	Pre-M	$\%\ near > 50 \wedge \%\ near + 1.8 \times \%\ mitotic > 100$	$\%\ near > 42 \wedge \%\ near + 1.8 \times \%\ mitotic > 100$	$\%\ mitotic$

Cells are first assigned to groups 1 and 5 and those remaining are assigned to groups 2-4. To compensate for the arbitrary thresholds (which may introduce discontinuity on the interfaces between the three main phases), the initial assignment to groups is then fine-tuned by clustering the contact distance distribution profiles of the cells to small clusters (k-means, k=number of cells / 10) and reassigning cells in each cluster to the majority vote of that cluster. This resulted in reassigning 5.7% and 8.2% of the cells in the diploid and haploid datasets, respectively, with almost all (>99.8%) re-assignments involving adjacent groups.

To test the stability of our phasing procedure among the different chromosomes we compared the positions of cells by phasing using disjoint sets of chromosomes with roughly the equivalent length (**Extended Data Fig. 7c**, 1st set: chromosomes 2, 3, 5, 6, 9, 10, 12, 15, 17 and 19, 2nd set: chromosomes X, 1, 4, 7, 8, 11, 13, 14, 16, and 18). Phasing positions determined by both sets largely concur, with most of the differences concentrated

on the interfaces between G1 and early S, or early S late S/G2 groups. The positions of only 38 out of the 1942 cells participated in both sets (<2) differ by more than 10%.

To perform the non-linear dimensionality reduction on the 2i diploids' contact distance profiles (**Extended Data Fig. 4e**), spectral embedding based on the above logarithmic bins (discarding the first <1Kb distance bin) was used to project the cells onto a two-dimensional plane while preserving local similarities. Specifically, for each two cells we computed the distance between their discretized decay distributions as:

$$d_{i,j} = D_{KL}(Cell_i, Cell_j) + D_{KL}(Cell_j, Cell_i)$$

We then generated the adjacency matrix of the k-NN graph (k=7), and used the 2nd and 3rd-smallest eigenvectors of the graph Laplacian as the projection axes.

Pooled contact maps

Contacts from single cell maps were pooled together to generate aggregated maps. We used the total number of contacts when creating ensemble-like maps, e.g. for the pool of all cells and the phase groups, and distinct contacts when creating contact maps comprising a few dozen cells (e.g. **Fig. 1h**, **Fig. 3b**). To normalize the pooled maps (**Extended Data Figs. 3a and 8h**), to compare pooled contacts around epigenetic landmarks (**Fig. 3e**), and to compare *cis* contact enrichment over a background contact distribution (**Fig. 4h, Extended Data Fig. 10e-f**), we sampled a randomized ensemble Hi-C map[26] and compared contact distributions in the observed and randomized data using the Shaman tool (https://bitbucket.org/tanaylab/shaman). Briefly, we shuffled contacts using a Markov Chain Monte Carlo-like approach, first within each chromosome and then genome-wide, such that the primary factors that define contact distributions are preserved - the marginal coverage and contact distance distribution - but any compartment or TAD structure that may be present is not retained. The resulting expected ensemble map has an identical number of contacts for each locus, and identical probability for a contact at a given genomic distance, as in the observed map. We generated shuffled maps from the pools of 2i diploids single-cells and the pool of 2i and serum haploids single-cells.

Insulation, domain and border calling and domains initial A/B classification

The insulation of a locus (**Supplementary Fig. 1**) corresponds to depletion of contacts in the "a" region. We calculate an insulation score by considering a distance around the locus (scale) and comparing the total number of contacts that violate insulation (in region *a*) with the total number of contacts around the locus (in regions *a*, b_1 and b_2). In both counts contacts distanced less than 1Kb from the diagonal are ignored (these are mostly non-digested contacts). The negative log-ratio of these counts correlates positively with strong insulation. We calculated insulation on the pooled contact maps in 1Kb resolution, using a

scale of 300Kb. Domains were then identified as contiguous regions in which insulation score is below the 90% quantile of the genome-wide distribution. Domains shorter than 20Kb or longer than 4Mb and domains containing a non-mappable region longer than 25kb were discarded, resulting in 2894 domains (or 2649 domains for the haploid pool of cells).

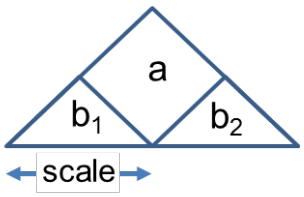

Supplementary Figure 1: Locus insulation

The initial assignment of domains to the A and B compartments was done by k-means clustering (K=2) the inter-domain contact profile, using only inter-chromosomal (*trans*) contacts, and computing log2 ratio of observed and expected (based on genomic length) inter-TAD contacts[20]. Domains in each cluster exhibit distinct epigenetic and time of replication signatures (**Extended Data Fig. 3d-e**) pointing us to assign the 1221 domains in cluster 1 to the B-, inactive-compartment and 1673 domains in cluster 2 to the A-, active compartment (haploids had 1353 A- and 1296 B-domains).

Domain borders were called from the insulation profile of the pooled map by identifying highly insulating regions between domains (insulation above the 90% quantile) and selecting in each element the 1KB with highest insulation score. To calculate the cell mean insulation over a set of borders *B* (either all borders as in **Fig. 3a** or a subset of borders as in **Fig. 3b**) the total number of border violating contacts is compared to the total number of contacts around the border. Denoting $A[b]$ as the number of contacts in the *a* region of border *b* (**Supplementary Fig. 1**) and similarly $B_1[b]$ and $B_2[b]$:

$$INS_B = log_2 \frac{\sum_{b \in B} A[b] + B_1[b] + B_2[b]}{\sum_{b \in B} A[b]}$$

To cluster borders by their insulation profile across the inferred cells phasing (**Fig. 3b**) cells were divided to 20 slices (100 cells in each slice grouped according to phasing), insulation was calculated per border and slice and the resulting 20 length border insulation profiles were clustered (k=4). **Fig. 3b** shows per cell (and not per slice) the mean insulation over each of the resulting clusters.

Inter-chromosomal alignment

The head-to-head alignment of chromosomes in single-cell mitotic Hi-C maps, likely represents late telophase or very early G1 nuclei (**Extended Data Fig. 4b**). To quantify the degree of head-to-head alignment of the chromosomes of each cell, we extracted trans-chromosomal contacts and scaled the coordinates of the contacting fends by the length of

their respective chromosomes. Alignment was then approximated using the Pearson correlation between the two scaled fend coordinate vectors (**Fig. 2g**).

A/B compartment score

Intra-chromosomal, inter-domain contacts were classified according to the compartment association of the contacting domains into A-A, A-B and B-B. Contacts within domains less than 2Mb apart were discarded. We summarized the statistics of observed total compartment contact per cell as (O_{AA}, O_{AB}, O_{BB}). The compartment score of a cell is the depletion of A-B contacts over the count expected by the marginal distribution of A or B contacts:

$$T = O_{AA} + O_{AB} + O_{BB} \qquad P(A) = \frac{2O_{AA} + O_{AB}}{T} \qquad P(B) = \frac{2O_{BB} + O_{AB}}{T}$$

$$CompScore = log_2 \frac{2 \cdot P(A) \cdot P(B) \cdot T}{O_{AB}}$$

Analyzing CTCF loops

We followed these steps to generate a set of loops:

- Genomic regions with strong CTCF ChIP-seq[15] signal were screened (50 bp regions on which either of the two ChIP-seq replicates genome-wide quantile is larger than 99%)
- Strong CTCF motifs were screened (Motif strength > 99.988% of the genome-wide 50 bp regions quantiles distribution)
- Each 50bp window was classified as *C* (only ChIP), *F* (ChIP + forward motif), *R* (ChIP + reverse motif) or *B* (ChIP + forward and reverse motif).
- Each ChIP-supported motif is classified by its upstream and downstream (200Kb) mean time of replication (ToR) as early (if mean ToR is positive) or late (if mean ToR is negative), resulting in the following anchor counts (discarding 116 loops with missing ToR information):

Upstream ToR	Downstream ToR	Denoted	Count
Early	Early	EE	55,778
Early	Late	EL	2,459
Late	Early	LE	2,598
Late	Late	LL	10,278

- Convergently oriented ChIP-supported motifs (B/F anchor upstream to a B/R one) distanced 200Kb-1Mb from each other were considered as loop candidates (total of 760,712)

- Loop candidates were further filtered by coverage enrichment in the normalized pool of 2i diploids contact map, requiring contact enrichment score higher than 60 within a 20x20Kb window centered on the loop, resulting with 61,796 loop candidates
- Loop foci enrichment (number of contacts in a 20x20Kb vs. 60x60Kb window centers on the loop) was calculated and the top quintile (20%, 12,361 loops) was selected.
- Overlapping loops (with overlapping 60x60Kb window center on the loop) were filtered, resulting in a final set of 2036 loops, with the following anchors classification:

1st anchor	2nd anchor	Denoted	Count
EE	EE	Early-Early	762
EE	LL	Early-Late	161
LL	EE	Late-Early	123
LL	LL	Late-Late	456
Mixed (EL/LE)	Mixed (EL/LE)	Mixed	534

Loop foci enrichment (**Fig. 3e**) quantifies how concentrated contacts are around a loop. We calculate the ratio between contacts in a small window (20x20kb) centered on the loop and contacts in a larger window (60x60kb), normalizing by the expected ratio if contacts were uniformly distributed (1/9). To get a mean loop foci enrichment over a group of loops, the sum of contacts in all small windows is compared with the sum of contacts in the larger ones.

Spatial analysis of contact distribution around loops (**Fig. 3f**) was performed by grouping observed and shuffled contacts in a 50x50kb window around loop anchors into 3Kb or 14Kb square bins (higher resolution of 3Kb bins is only possible for the 3 large group of cells: G1, Early-S and Late-S/G2), and color coding according to the per-bin log fold ratios over shuffled-data statistics.

Domain condensation

The condensation level of a domain is quantified by the mean contact distance of contacts within the domain. To ensure domain coherence for condensation analysis (**Fig. 3g**) we used a more fine-grained domain definition with a higher threshold on the insulation (85 percentile for calling domains, instead of 90) resulting in 3,683 domains, out of which 3,622 had time of replication information. Each domain was classified by its mean time of replication and its length, resulting in the following groups of domains:

		Domains length range			
	mean ToR (mT)	**1-244K**	**244-490K**	**490-980K**	**980-1500K**
Early	mT > 0.84	399	439	223	24
Mid-Early	0 < mT < 0.84	401	361	267	47
Mid-Late	-0.66 < mT < 0	142	174	218	116
Late	mT < -0.66	113	128	223	99
Total		1055	1102	931	286

As expected from earlier reports, domains length was correlated with time of replication, but sufficient statistics was available for analysis in less populated bins:

	1-244K	**244-490K**	**490-980K**	**980-1500K**
Early	36.77%	40.46%	20.55%	2.21%
Mid-Early	37.27%	33.55%	24.81%	4.37%
Mid-Late	21.85%	26.77%	33.54%	17.85%
Late	20.07%	22.74%	39.61%	17.58%

Computing distributions of single-cell compartment association scores

In order to analyze the compartmentalization behavior of domains in a population of single cells, we defined two scores for each domain:

A-score: quantifies the tendency of a domain to interact with A domains. Calculated solely from *trans*-chromosomal contacts of an ensemble-like contact map (pool of singles or bulk Hi-C).

A-association score: quantifies the interaction with A domains of a given domain in a specific cell. Calculated from *cis*-chromosomal contacts (> 2Mb) of a single-cell.

To compute A-score we first calculate the fraction of *trans* contacts each domain has with A domains, which we term *A-fraction* (see above for details how domains are clustered to the A and B groups). We then calculate for each domain the mean A-fraction of the domains it interacts with in *trans* (considering the number of contacts between the domains as weights), which results in an A-score for each domain. (see comparisons of A-scores from different maps in **Extended Data Fig. 9a**).

Because of the sparsity of *trans* contacts in a single-cell contact map, we used *cis* contacts to explore the dynamics of compartments behavior at a single-cell level. A-association scores per single-cell and domain, are computed using *cis* contacts at distances above 2 Mb. We first filtered domains whose A-score was calculated by at least 20 *trans* contacts

(discarding 90 out of 2649 haploid domains and 5 out of 2894 diploid domains). Next, for each single-cell, we only used domains with more than three contacts with at least two other domains. We then sampled two of the interacting domains and took their mean A-score as the A-association score of the domain in that cell. By sampling two domains we control for possible differences in A-score variance that are due to differences in marginal TAD coverage.

To study haploid A-scores, while maximizing consistency with the diploid system, we computed for each haploid domain, the overlapping diploid domains and calculated their weighted mean (diploid) A-score. We then defined a critical value of weighted A-score means to re-define A/B labels in haploids, using a threshold that maximizes the similarity between these A/B labels and the labels derived by standard compartment clustering as performed for diploids. Given these revised A/B labels for haploid TADs, we repeated the procedure described above (computing haploid A-score and haploid A-association) using haploid single cell maps. Note that in this way we used the diploid compartments solely for bootstrapping the haploid process.

Ranking domains by A-association score distributions and assigning to pseudo-compartments

For unsupervised analysis, domains were clustered by the distribution of their A-association scores in each group of cells (k-means, k = 20, **Extended Data Fig. 9b**). Given the absence of clusters showing bimodal distributions, domains were ordered by their mean A-association score at the late S to G2 group, where compartmentalization is peaking (**Fig. 3b**). Pseudo-compartments were then defined by discretizing the ranking into 20 equal size groups.

Creating normalized pseudo-compartment interaction maps

We derived an observed pseudo-compartment interaction map from the contact map pooling cells in each cell-cycle phase by summing the number of contacts between domains in each pseudo-compartment, separately for *cis*- (> 2Mb) and for *trans*-chromosomal contacts. To derive the *cis*- and *trans*-chromosomal contact enrichments (**Fig. 4h-l and Extended Data Fig. 9f**) we took the log ratio of the observed values and the expected contingency table generated from the observed marginal pseudo-compartment coverage across all three groups**.** For the *cis* pseudo-compartment maps in **Extended Data Fig. 9e**, we took the log of the element-wise ratio between the observed pseudo-compartment map and an expected pseudo-compartment map summed from the shuffled pool contact map.

Epigenetic annotations

Track	Source	Usage	Processing
Time of replication	Repli-chip of ES-D3[16] (rep 1)	Calculating repli-score and classifying TADs	Mean value on regions (TADs, upstream/downstream to landmarks,10kb around a fend for repli-score)
Haploid RNA-seq	In-house (experimental details above)	4j	Log2(mean of 2 replicates over TAD)
Diploid RNA-seq	In-house (experimental details above)	Ext 3e, Ext 10h	-log2(1 – max(reps max percentile)
H3K4Me1	ChIP-seq of ES-Bruce4[16]	4j	Mean of 2 replicates over TAD
H3K4me3	ChIP-seq of ES-Bruce4[16]	4j	Mean of 2 replicates over TAD
H3K4me3	ChIP-seq of ES-Bruce4[16] (rep 1)	Ext 3e	Fraction of TAD with peaks (peak = score > 99% percentile)
H3K27me3	ChIP-seq of ES-Bruce4[16]	Ext 3e	Mean of 2 replicates over TAD
LaminB1	mESC LaminB1 DamID[18]	4j, Ext 3e	mean LaminB1 value over TAD
CTCF	ChIP-seq of ES-Bruce4[16]	Fig 3d-e	Details on loops section above

Mapping and filtering before 3D modelling

Since structural modelling is sensitive to low levels of noise, haploid G1 cells were processed using stringent contact filtering to remove contacts that are more likely to be technical artefacts. We first used HiCUP[27], applying a di-tag size selection from 50 bps to 850bps, for mapping di-tags and filtering out common Hi-C artefacts. Putative PCR duplicates were not removed by HiCUP, instead the filtered data was then passed a new tool (SiCUP) for further single-cell Hi-C specific filtering. We removed reads mapping to the Y chromosome, to short restriction fragment (less than 21bps) and to regions defined as problematic by ENCODE. We also filtered reads mapping to fragment ends forming multiple interactions in one percent or more of the datasets. To avoid potential artefacts we removed singleton di-tags. In haploid G1 cells there is only one copy of the genome, hence after removal of PCR-duplicates each observed fragment end should be in contact with at most one other fragment end. Consequently, multiple contacts from the same fragment were removed entirely. An exception to this was when a fragment end (A) interacted with two other fragments ends (B and C) which were close together (defined here as when B and C were within 20 MboI fragments). In such instances the strand orientation of the reads mapping to B and C were typically the same, to a degree not expected by chance (as defined by a chi-squared test when evaluating the whole dataset). We reasoned that in such instances these apparently distinct interactions were in fact derived from one initial Hi-C interaction. Consequently, when this was observed, not all the

di-tags were discarded. Instead, if the Hi-C interaction was in trans, a random di-tag was discarded. Alternatively, when the Hi-C interaction was in cis, the di-tag representing the shortest Hi-C interaction was retained.

We also filtered out unsupported contacts. For each cell, using the filtered contacts, we first derived a connectivity graph of the genome. Nodes of the graph represented 1Mb segments of the genome, and each edge represented a single contact mapped onto 1 Mb resolution, so any two nodes of the graph might be connected by more than one edge. We defined a contact as unsupported if upon deletion of that contact, the shortest path connecting its two end nodes would be longer than 3 edges. These unsupported contacts (median 1.06% of contacts, **Extended Data Fig. 10a**) were removed from the sc-HiC libraries before 3D modelling.

Polymer model for whole-genome modelling

We modeled chromatin as a simple non-overlapping beads-on-a-string polymer[12] subject to data derived constraints. The energy function consists of a bond potential that ensures the connectivity of the polymer chain within chromosomes, a second term that prevents overlaps of chromatin and a third term that enforces the observed contacts as distance constraints with different contact points for each cell. Note that no other physical parameter, e.g. the overall shape or size of the nuclear envelope, is constrained by our modelling approach, hence the overall three-dimensional shape of the entire genome is purely determined by the filtered and supported chromosome contacts in the corresponding single-cell Hi-C library. We implemented this coarse-grained polymer model to be used with the GROMACS 5.0.6 molecular dynamics package[28]. The energy function and the exact values of the model parameters are listed in the Supplementary Material. Briefly, the exclusion energy term is a harmonic function for distances below d_0 with a force constant k^{excl}, and the bond and constraint energy terms are defined by a flat-bottomed harmonic function with no energy penalty for distances between d_0 to d_1, and a harmonic potential with a force constant k outside this range which turns into a linear function for distances greater than d_2. 3D models were optimised using a simulated annealing protocol, using a piecewise linear temperature profile, and different initial conditions to assess convergence robustness.

Quality control of 3D models

To avoid underdetermined models, we only considered models that were computed using at least 10,000 filtered contacts. The root mean square distance (RMSD, the smallest possible Euclidean distance) of models, indicating the reproducibility of models, as a function of the number of contacts is shown in **Extended Data Fig. 10d**. We also

discarded models with high numbers of violated constraints. For this, we considered a constraint violated when its distance was greater than d_2 (constrained distances are expected to be greater than d_1 by construction, due to thermal fluctuations). At 1 Mb resolution there were no violated constraints for 171 of the 190 cells (**Extended Data Fig. 10b**), and the fraction of violated constraints strongly correlated at the 500 kb and 100 kb resolutions (Pearson R = 0.96). For further analysis, we selected 127 cells that on median had no more than 0.5% violated constraints at the 500 kb resolution and no more than 0.1% violated constraints at the 100 kb resolution (shown as black dots in **Extended Data Fig. 10c**). We further discarded one cell that had more than 10% of a chromosome missing, resulting in 126 ordered G1 cells with high-quality models for downstream analysis.

We tested robustness to the initial conditions by using permuted chromosomes along a spiral as well as folded structures of other nuclei as the initial chromatin conformation. Results were robust to changes to the initial conditions, indicating the convergence of the simulations, which was measured by computing the distribution of the root-mean-square-distance (RMSD) between aligned models of the same cell compared to different cells (**Extended Data Fig. 10e**). Models at different resolutions were compared to one another by downsampling the higher resolution structures to 1 Mb, and scaling the nuclear radius of the model to the nuclear radius of the 1 Mb model. The downsampled models computed at different resolutions were consistent at 1 Mb resolution. Models were also robust when scaling the model parameters by a factor of half or two.

Cross validation

To test the robustness of our 3D modelling approach to missing contacts, we performed a cross validation test. For each cell, we identified the 5 most strongly interacting chromosome pairs, measured by the number of contacts between the two chromosomes. For each of these 5 chromosome pairs, we removed all *trans* contacts between that chromosome pair and recomputed a structure model for that cell (we only delete interactions between one chromosome pair at a time). We computed the distance distribution of the removed constraints in the models computed with those constraints removed (**Extended Data Fig. 10f** blue line), and compared it to their distance distribution in randomly selected cells (control, **Extended Data Fig. 10f** green line). The distances of these removed contacts are noticeably shorter in their corresponding model than they are in randomly selected other cell, indicating that the proximity of the chromosome pair is preserved. This suggests that these sparse datasets contain sufficient information about chromosome level interactions for robust structural modelling. This is probably due to their indirect coupling through their contacts with their neighbouring chromosomes. In

comparison, the distances of the unsupported contacts filtered out before modelling (**Extended Data Fig. 10f** light blue line) were much more similar to the control, indicating that most of those interactions are likely noise.

Chromosome decondensation

We grouped the 126 cells into 7 time groups in G1 (**Extended Data Fig. 10h**). As the chromatin structure varied most in early G1, we used 4 time groups in the first quarter of the 126 G1 ordered cells, and 1 group for each of the remaining three quarters. We computed the nuclear radius from its radius of gyration. As an indicator of nucleus sphericality, we also computed the inertia ellipsoid of the nucleus. The detailed description of how these quantities are computed can be found in the Supplementary Material. We noted that although the nuclear lamina is not modelled by the force field, the models turn out to be near spherical ($a \approx b \approx c$) and roughly the same size (**Extended Data Fig. 10g**, nucleus a/c ratio). We also noted that low mappability regions tend to be more flexible and uncertain in their position in the computed models, illustrated by the unconstrained region around chrX:30Mb (the white chromatin region looping out of the models in **Extended Data Fig. 10e)**. To illustrate changes in the overall chromatin structure, we selected an M-phase and a late (118^{th} of the 126 ordered cells) G1 cell. We plotted the whole genome structure and a karyotyped image at 100 kb resolution (**Fig. 5a**). The structure models were visualised and aligned using VMD[29] 1.9.1, the images were rendered using PovRay 3.7 (http://www.povray.org). The colour scheme used for the chromosomes was chosen to provide maximum contrast[30].

To quantify the decondensation of chromosomes during G1, we fitted an ellipsoid to each chromosome of every model and averaged the values over all models of the same cell. As a measure of sphericality, we used the longest-to-shortest semiaxis ratio (**Extended Data Fig. 10g**, chromosome a/c ratio) together with the middle-to-shortest semiaxis ratio (**Extended Data Fig. 10g**, chromosome b/c ratio). Larger a/c ratios together with $b/c \approx 1$ in early G1 indicate rod-like structures that decondense into a more spherical structure as a/c decreases to $a \approx b \approx c$. We plotted the distribution of all chromosome a/c ratios over cells in the 7 time groups with illustrating examples of chromosome 1 from each time group in **Fig. 5b** of the Main text.

3D organisation of compartments

To investigate the spatial organisation of compartmentalisation, we assigned compartment labels to the beads using a majority vote. Beads with no compartments were excluded from further analysis. As an indicator of local decompaction of chromatin, we computed the average distance of neighbouring chromatin segments of the same compartment,

normalised by the d_1^{bond} bond length parameter. We computed the average compartment decompaction values for each model, and averaged them across all 3D models of the same cell. The distribution over all cells in the 7 time groups is shown in **Fig. 5c-d**. We tested if the mean A and B compartment decompaction values came from the same distribution using Mann–Whitney statistics.

We also computed the average radial positioning of the compartments. For each bead, we computed its radial position as a volume fraction, increasing linearly between the nucleus centre-of-mass (0) and the nuclear radius (1) in the volume enclosed by a sphere of that distance radius from the nucleus centre. We averaged the radial position values of all beads of the same compartment, and across all 3D models of the same cell. We plotted the distribution of the radial positions across the cells in the 7 time groups in **Fig. 5e-f**. We tested if the mean A and B compartment radial position values came from the same distribution by performing a Mann–Whitney test on each time group.

Testing the enrichment of compartment co-localisation between pairs of pseudo-compartments in long *cis* (> 2 Mb genomic distance) or *trans* was done separately. For this analysis, we defined two beads in contact if their distance was within 10% of the nucleus diameter. For any two pseudo-compartments, we counted the contacting bead pairs in long *cis* or *trans*, for which one bead belonged to one pseudo-compartment, while the other bead belonged to the other pseudo-compartment. We averaged these counts over all models of all cells in the 7 time groups of G1, and rounded them down to the nearest integer, resulting the observed counts. We shuffled the bead contacts while keeping the number of contact beads of each compartment constant, resulting the expected counts. We plotted the $\log_2$(observed/expected) ratios between any two pseudo-compartments as a matrix (**Fig. 5g-h**).

Nuclear Organiser Region clustering

For each chromosome, we used the first constrained bead as the pericentromeric region closest to the centromere. Chromosomes were divided into two groups, Nucleolar Organiser Region (NOR) chromosomes (chromosomes 11, 12, 15, 16, 18 and 19), and other chromosomes[19]. We computed all pairwise distances between the pericentromeric regions within these two groups normalised by the nucleus diameter, and plotted the distribution of the top one third of these distances across all models of cells for each time group (**External Data Fig. 10i**). We averaged these distances for each model and each cell, and tested if the mean of the top third shortest centromere distances came from the same distribution by performing a Mann–Whitney test on each time group.

Data Availability

All data reported in this study is available at GEO GSE94489.

Code Availability

Additional analysis files and scripts are available from our website or upon request.

References

1. Paweletz, N. Walther Flemming: pioneer of mitosis research. *Nat. Rev. Mol. Cell Biol.* **2**, 72–75 (2001).

2. Lieberman-Aiden, E. et al. Comprehensive mapping of long-range interactions reveals folding principles of the human genome. *Science* **326**, 289–93 (2009).

3. Sexton, T. et al. Three-dimensional folding and functional organization principles of the Drosophila genome. *Cell* **148**, 458–72 (2012).

4. Nora, E. P. et al. Spatial partitioning of the regulatory landscape of the X-inactivation centre. *Nature* **485**, 381–5 (2012).

5. Dixon, J. R. et al. Topological domains in mammalian genomes identified by analysis of chromatin interactions. *Nature* **485**, 376–80 (2012).

6. Sofueva, S. et al. Cohesin-mediated interactions organize chromosomal domain architecture. *EMBO J.* **32**, 3119–29 (2013).

7. Rao, S. S. P. S. P. et al. A 3D Map of the Human Genome at Kilobase Resolution Reveals Principles of Chromatin Looping. *Cell* **159**, 1665–1680 (2014).

8. Zuin, J. et al. Cohesin and CTCF differentially affect chromatin architecture and gene expression in human cells. *Proc. Natl. Acad. Sci. U. S. A.* **111**, 996–1001 (2014).

9. de Wit, E. et al. CTCF Binding Polarity Determines Chromatin Looping. *Mol. Cell* **60**, 676–684 (2015).

10. Flavahan, W. A. et al. Insulator dysfunction and oncogene activation in IDH mutant gliomas. *Nature* **529**, 110–114 (2016).

11. Naumova, N. et al. Organization of the mitotic chromosome. *Science* **342**, 948–53 (2013).

12. Nagano, T. et al. Single-cell Hi-C reveals cell-to-cell variability in chromosome structure. *Nature* **502**, 59–64 (2013).

13. Nagano, T. et al. Comparison of Hi-C results using in-solution versus in-nucleus ligation. *Genome Biol.* **16**, 175 (2015).

14. Pope, B. D. et al. Topologically associating domains are stable units of replication-timing regulation. *Nature* **515**, 402–405 (2014).

15. Stamatoyannopoulos, J. A. et al. An encyclopedia of mouse DNA elements (Mouse ENCODE). *Genome Biol.* **13**, 418 (2012).

16. Boettiger, A. N. et al. Super-resolution imaging reveals distinct chromatin folding for different epigenetic states. *Nature* **529**, 418–422 (2016).

17. Peric-Hupkes, D. et al. Molecular maps of the reorganization of genome-nuclear lamina interactions during differentiation. *Mol. Cell* **38**, 603–13 (2010).

18. Dileep, V. et al. Topologically-associating domains and their long-range contacts are established during early G1 coincident with the establishment of the replication timing program. *Genome Res.* **25**, 1104–1113 (2015).

19. Britton-Davidian, J., Cazaux, B. & Catalan, J. Chromosomal dynamics of nucleolar organizer regions (NORs) in the house mouse: micro-evolutionary insights. *Heredity*. **108**, 68–74 (2012).

20. Ramani, V. et al. Massively multiplex single-cell Hi-C. *Nat. Methods* **14**, 263–266 (2017).

21. Stevens, T. J. et al. 3D structures of individual mammalian genomes studied by single-cell Hi-C. *Nature* **544**, 59-64 (2017).

22. Flyamer, I. M. et al. Single-nucleus Hi-C reveals unique chromatin reorganization at oocyte-to-zygote transition. *Nature* **544**, 110–114 (2017).

23. Leeb, M. & Wutz, A. Derivation of haploid embryonic stem cells from mouse embryos. *Nature* **13**, 1–5 (2011).

24. Leeb, M., Perry, A. C. F. & Wutz, A. Establishment and Use of Mouse Haploid ES Cells. *Curr. Protoc. Mouse Biol.* **5**, 155–85 (2015).

25. Langmead, B. & Salzberg, S. L. Fast gapped-read alignment with Bowtie 2. *Nat Methods* **9**, 357–359 (2012).

26. Olivares-Chauvet, P. et al. Capturing pairwise and multi-way chromosomal conformations using chromosomal walks. *Nature* **540**, 296-300 (2016).

27. Wingett, S. et al. HiCUP: pipeline for mapping and processing Hi-C data. *F1000Research* **4**, 1310 (2015).

28. Berendsen, H. J. C., van der Spoel, D. & van Drunen, R. GROMACS: A message-passing parallel molecular dynamics implementation. *Comput. Phys. Commun.* **91**, 43–56 (1995).

29. Humphrey, W., Dalke, A. & Schulten, K. VMD: Visual molecular dynamics. *J. Mol. Graph.* **14**, 33–38 (1996).

30. Green-Armytage, P. A Colour Alphabet and the limits of colour coding. *JAIC-Journal Int. Colour Assoc.* **10**, 1–23 (2010).